SIAM J. NUMER. ANAL.
Vol. 59, No. 2, pp. 1117–1139

A MIXED APPROACH TO THE POISSON PROBLEM WITH LINE SOURCES*

INGEBORG G. GJERDE†, KUNDAN KUMAR†, AND JAN M. NORDBOTTEN†

Abstract. In this work we consider the dual-mixed variational formulation of the Poisson equation with a line source. The analysis and approximation of this problem is nonstandard, as the line source causes the solutions to be singular. We start by showing that this problem admits a solution in appropriately weighted Sobolev spaces. Next, we show that given some assumptions on the problem parameters, the solution admits a splitting into higher- and lower-regularity terms. The lower-regularity terms are here explicitly known and capture the solution singularities. The higher-regularity terms, meanwhile, are defined as the solution of an associated mixed Poisson equation. With the solution splitting in hand, we then define a singularity removal–based mixed finite element method in which only the higher-regularity terms are approximated numerically. This method yields a significant improvement in the convergence rate when compared to approximating the full solution. In particular, we show that the singularity removal–based method yields optimal convergence rates for lowest-order Raviart–Thomas and discontinuous Lagrange elements.

Key words. singular elliptic equations, finite elements

AMS subject classifications. 35J75, 65M60

DOI. 10.1137/19M1296549

1. Introduction.

Let $\Omega \subset \mathbb{R}^3$ be a bounded 3D domain with smooth boundary $\partial\Omega$. Let Λ be a differentiable manifold with topological dimension 1. We denote the reference domain of Λ as $S = (0, L) \subset \mathbb{R}^1$. Furthermore, we denote the mapping $\Xi : S \to \Omega$ as $\boldsymbol{\lambda}$. Thus, Λ can be represented by the parametrization $\boldsymbol{\lambda} = [\xi(s), \tau(s), \zeta(s)]$ so that $\Lambda = \{\boldsymbol{\lambda}(s) : 0 < s < L\} \subset \Omega$. For simplicity, we assume $\|\boldsymbol{\lambda}'(s)\| = 1$ so that the arc-length and coordinate s coincide. We consider in this work the mixed Poisson problem with a line source on Λ: Find u and $\mathbf{q}$ solving

$$\mathbf{q} + \kappa \nabla u = 0 \qquad \text{in } \Omega, \tag{1.1a}$$

$$\nabla \cdot \mathbf{q} = f\, \delta_\Lambda \qquad \text{in } \Omega, \tag{1.1b}$$

$$u = u_0 \qquad \text{on } \partial\Omega, \tag{1.1c}$$

where $f \in C^2(\bar{\Omega})$ denotes the line source intensity, $\kappa \in L^\infty(\Omega)$ a symmetric matrix with uniformly bounded eigenvalues, $u_0 \in C^2(\bar{\Omega})$ the boundary data, and δ_Λ a Dirac line source concentrated on Λ. We note that by the superposition principle, (1.1a)–(1.1c) could be extended so that Λ could be a collection of 1D curves Λ_i; this would allow for, e.g., branching geometries.

Let further Ω_R denote a tubular neighborhood around Λ with a given radius R,

$$\Omega_R = \{\mathbf{x} \in \Omega : \ r(\mathbf{x}) < R\}, \tag{1.2}$$

Here, $r = \text{dist}(x, \Lambda)$ denotes the distance from a point $x \in \Omega$ to the closest point on Λ, as illustrated in Figure 1.1. We assume Λ is such that for R small enough, each

*Received by the editors October 30, 2019; accepted for publication (in revised form) October 26, 2020; published electronically April 29, 2021.
https://doi.org/10.1137/19M1296549
Funding: The work of the authors was supported by the Research Council of Norway project 250223.

†Department of Mathematics, University of Bergen, Bergen 5020, Norway (ingeborg@simula.no, kundan.kumar@uib.no, jan.nordbotten@math.uib.no).

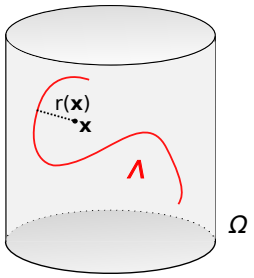

FIG. 1.1. *A 3D domain $\Omega \subset \mathbb{R}^3$ with an embedded line Λ, with $r(\mathbf{x}) = \operatorname{dist}(\mathbf{x}, \Lambda)$ denoting the distance of a point in Ω to the line.*

$\mathbf{x} \in \Omega_R$ has a unique closest point in Λ. The line source δ_Λ is then taken as the limit of a sequence of nascent Dirac functions of unit measure per arc length,

$$\delta_\Lambda = \lim_{\epsilon \to 0} \delta_\Lambda^\epsilon, \quad \delta_\Lambda^\epsilon(\mathbf{x}) = \begin{cases} \frac{1}{\pi \epsilon^2} & \text{for } \mathbf{x} \in \Omega_\epsilon, \\ 0 & \text{otherwise,} \end{cases} \tag{1.3}$$

where the limit is in the sense of distributions.

Models of the type (1.1a)–(1.1c) arise in a variety of applications. In geophysics, line sources have been used to model 1D steel components in concrete structures [38] and the interference of metallic pipelines and bore casings in electromagnetic modeling of reservoirs [48]. In the context of geothermal energy, line sources have been used to model the heat exchange between a well and the surrounding soil [3]. In reservoir engineering, coupled 1D-3D flow models (where (1.1a)–(1.1c) is coupled to a 1D flow equation on Λ) are used to model the flow between a well and a reservoir [13, 49, 1]. The same model has also been considered in the context of biological systems, where it has been used to model water flow through a root system [25, 27], blood and oxygen transport through the vascularized tissue of the brain [44, 22, 47, 18, 37], the efficiency of cancer treatment by hyperthermia [41], and the efficiency of drug delivery through microcirculation [12, 43].

In many of these applications, the flow equation (1.1a)–(1.1c) will be coupled to a transport equation (describing, for example, heat flow or the concentration of some chemical). For this reason, we consider herein the mixed variational formulation of (1.1a)–(1.1b). On discretization, this will yield a mixed finite element method, which is known to provide good approximations of the velocity field. In particular, it provides locally conservative approximations.

As we will see, the analysis and approximation of (1.1a)–(1.1b) is nonstandard, as the line source δ_Λ induces the solution to be singular. To be more precise, one has that δ_Λ induces a logarithmic-type singularity in u and a r^{-1}-type singularity in $\mathbf{q}$. Consequently, one has $\mathbf{q} \notin (L^2(\Omega))^3$. The analysis of (1.1a)–(1.1b) therefore requires nonstandard Sobolev spaces. From a numerical perspective, the singular nature of u and $\mathbf{q}$ makes them challenging to approximate.

In this work, we (1) prove the existence of a solution to (1.1a)–(1.1b) and (2) construct an efficient numerical method with which to approximate it. The existence of a solution is proved using a suitably weighted Sobolev space, similar to the ones used in [5, 11]. With these spaces, the proof follows by the generalized Lax–Milgram theorem together with a limit argument. As we will see, the analysis raises questions regarding the approximation properties of $\mathbf{q}$. For this reason, we extend our work from [21] to show that with some assumptions on the problem parameters, the solution

admits a splitting of the type

$$u = u_s + u_r, \quad \mathbf{q} = \mathbf{q}_s + \mathbf{q}_r, \tag{1.4}$$

where u_s and $\mathbf{q}_s$ denote explicitly known terms capturing the solution singularities and u_r and $\mathbf{q}_r$ denote higher-regularity remainder terms. The remainder terms are defined as the solution of an associated mixed Poisson equation. With the splitting in hand, we then formulate a solution strategy in which only u_r and $\mathbf{q}_r$ are approximated using a mixed finite element method. In contrast to the development in [21], this has the advantage of providing a locally mass conservative approximation. The full solution pair $(u, \mathbf{q})$ can then be reconstructed using (1.4). We will refer to this as the singularity removal–based mixed finite element method.

1.1. Relevant literature and our contribution. Several authors have contributed to the analysis of the Poisson equation with a line source. Of special relevance to our work, we mention the work of D'Angelo and Quarteroni in [16], where they proved the existence of a solution to the primal (nonmixed) variational formulation of (1.1a)–(1.1c). The proof relied on weighted Sobolev spaces similar to those known from the study of corner-point problems [6]. In [15], D'Angelo went on to study the finite element approximation of the problem. There, he found that the approximation converges suboptimally in the L^2-norm and fails to converge in the H^1-norm. Convergence can be improved by weighing the error norm, and optimal convergence rates can be retrieved by grading the mesh, i.e., by performing a particular refinement around the singularity. A similar result is known for the point source problem in 2D [17, 4]. In the context of applications, however, Λ may be a graph with nontrivial geometry and a large number of edges. The data set used in [23, Figure 4], as one example, consists of ∼3000 line segments representing the arterial and venous systems of the brain. For such data sets, it would be infeasible to construct suitably graded meshes. In this case, h-adaptivity could be used instead [2, 14]. This approach is similarly known to restore optimal convergence rates for singular functions but may be computationally expensive.

In the coupled 1D-3D flow model, the singular behavior of the solution makes it challenging to resolve the coupling condition for the flow equations on Ω and Λ. Köppl et al. in [31] proved that the convergence issues induced by the line source are local to Λ, meaning that it only impacts the approximation quality close to Λ. For the coupled 1D-3D flow model, this means that the numerical approximation will suffer pollution until the mesh size h is smaller than R (R being the original radius of, e.g., a blood vessel or well). We show in [20] that for uniform meshes, the finite element approximation of the coupled 1D-3D flow therefore requires a very fine mesh to converge.

Several strategies have been proposed in order to deal with the computational complexity this introduces. We refer the reader to the work of Kuchta et al. in [34] and Bærland, Kuchta, and Mardal in [7] for suitable preconditioners for the coupled 1D-3D problem. Holter, Kuchta, and Mardal in [24] then applied this preconditioner to simulate flow through the microcirculature found in a mouse brain. Koch et al. in [28] introduced a smoothing kernel to distribute the line source over a 3D subdomain. An alternative coupling scheme was introduced by Köppl et al. in [30, 32], where the source term was taken to live on the boundary of the inclusions. This idea was further developed in [13, 36]. The result is a 1D-(2D)-3D method where the dimensional gap has been reduced to 1, thus improving the approximation properties of the solution. However, this approach requires the 2D mesh for the boundary of the inclusions to be resolved in the 3D mesh for Ω; thus, one still requires $h \sim R$.

In [21], we consider a singularity removal–based method for the primal formulation of the Poisson problem with line sources. This method was found to enjoy improved approximation properties; in particular, it yields optimal convergence rates for lowest-order elements and removes the pollution around the line source. The singularity removal–based approach is extended in [20] to the coupled 1D-3D flow model; here, it was found to restore convergence for uniform meshes even when $R \ll h$.

The works cited so far have all been on the primal variational formulation of (1.1a)–(1.1c). Comparatively little work has been done that considers its mixed formulation (as an exception, we note the work of Notaro et al. in [42] in providing a mixed finite element discretization of the coupled 1D-3D flow model). A mathematical analysis of (1.1a)–(1.1c) is, however, to the best of our knowledge, still missing, as is the construction of a suitable numerical method with which to approximate the solution. The aim of this article is to fill this gap.

1.2. Overview of the paper. We start in section 2 by introducing the weighted Sobolev spaces. With these in hand, we then prove in section 3 the existence of a solution to the (dual-)mixed variational formulation of (1.1a)–(1.1c). The solution is shown to exist in a nonstandard space with poor approximation properties. For this reason, we proceed in section 4 to construct a solution splitting of the type (1.4), where the solution is split into higher- and lower-regularity terms. In section 5, we give the mixed finite element discretization of the problem. Here, we provide two different methods: the standard mixed finite element method that approximates the full solution pair $(u, \mathbf{q})$ and a singularity removal–based finite element method that approximates only the higher-regularity remainder pair $(u_r, \mathbf{q}_r)$. In section 6.1, we provide numerical evidence that the former method fails to converge in the standard L^2-norm. In section 6.1, we then show that the latter method, i.e., solving for the remainder pair $(u_r, \mathbf{q}_r)$, yields optimal convergence rates for lowest-order elements. We conclude by showing the results of applying the singularity removal–based mixed finite element method on a nontrivial geometry taken from the vascular network of a rat tumor.

2. Function spaces and notation. The purpose of this section is to introduce the weighted Sobolev spaces in which solutions to (1.1a)–(1.1c) belong. We start by giving the definition of the standard Sobolev spaces. Let $\mathrm{d}x$ denote the standard Lebesgue measure in $\mathbb{R}^3$, σ the σ-algebra on Ω, and $(\Omega, \sigma, \mathrm{d}x)$ the usual Lebesgue measure space. Letting $L^2(\Omega)$ denote the space of square integrable functions on $(\Omega, \sigma, \mathrm{d}x)$, the Sobolev space $H^m(\Omega)$ can be defined as

$$H^m(\Omega) = \{u \text{ measurable } : D^\beta u \in L^2(\Omega) \text{ for all } |\beta| \leq m\},$$

equipped with the inner product

$$(u, v)_{H^m(\Omega)} = \sum_{|\beta| \leq m} (D^\beta u, D^\beta v),$$

where $(\cdot, \cdot)$ denotes the L^2-inner product $(u, v)_\Omega = \int_\Omega uv \, \mathrm{d}x$, β is a multi-index, and $D^\beta u$ denotes the corresponding distributional partial derivative of u. A subscript $H_0^m(\Omega)$ is used to denote the subspace of $H^m(\Omega)$ with zero trace on the boundary. Next, let $H(\mathrm{div}; \Omega)$ be given as

$$H(\mathrm{div}; \Omega) = \{\mathbf{q} \in (L^2(\Omega))^3 : \nabla \cdot \mathbf{q} \in L^2(\Omega)\},$$

equipped with the inner product

$$(\mathbf{q}, \mathbf{v})_{H(\mathrm{div};\Omega)} = (\mathbf{q}, \mathbf{v}) + (\nabla \cdot \mathbf{q}, \nabla \cdot \mathbf{v}).$$

Let $r(\mathbf{x}) = \operatorname{dist}(\mathbf{x}, \Lambda)$ denote the distance of a point $\mathbf{x} \in \Omega$ to Λ. Formally, the function $r(\mathbf{x})$ behaves as the r-component of a cylindrical coordinate system around the center line Λ. As we will see in section 4, the line source δ_Λ introduces a r^{-1}-type singularity in $\mathbf{q}$. For this reason, $\mathbf{q}$ fails to belong to $L^2(\Omega)$; consequently, it also fails to belong to the standard $H(\mathrm{div}; \Omega)$ space. As we will see, the solution $\mathbf{q}$ will instead belong to a weighted H-div space. Let $\alpha \in \mathbb{R}$, and take $L^2_\alpha(\Omega)$ to denote the weighted space

$$L^2_\alpha(\Omega) := \left\{ u \text{ measurable } : \int_\Omega (r^\alpha u)^2 \, \mathrm{d}x < \infty \right\}.$$

This is a Hilbert space equipped with the inner product

$$(u, v)_{L^2_\alpha(\Omega)} = \int_\Omega r^{2\alpha} uv \, \mathrm{d}x.$$

Formally, the value of α controls how singular the function is allowed to be. Increasing α leads to an increase in the space $L^2_\alpha(\Omega)$; i.e., letting $\alpha_1 < \alpha_2$, one has $L^2_{\alpha_1}(\Omega) \subset L^2_{\alpha_2}(\Omega)$. Next, by an application of Cauchy–Schwarz, we obtain

$$|(u, v)| = |(r^\alpha u, r^{-\alpha} v)| \leq \|u\|_{L^2_\alpha(\Omega)} \|v\|_{L^2_{-\alpha}(\Omega)} \quad \forall\, u \in L^2_\alpha(\Omega),\, v \in L^2_{-\alpha}(\Omega), \tag{2.1}$$

meaning that (u, v) is bounded for $u \in L^2_\alpha(\Omega)$ and $v \in L^2_{-\alpha}(\Omega)$. Furthermore, the dual space of $L^2_\alpha(\Omega)$ coincides with $L^2_{-\alpha}(\Omega)$ [39, Lemma 2.1.7].

For $\alpha \in (-1, 1)$, the weights r^α are said to be *Muckenhoupt*, and we have the imbedding $L^2_\alpha(\Omega) \hookrightarrow L^1(\Omega)$ [46, section 1.2.2]. The space $L^2_\alpha(\mathrm{div}; \Omega)$ then admits properties such as density of smooth functions $C^\infty_0(\Omega; \mathrm{d}x)$. For general α, the properties of L^2_α are best understood in the context of measure theory. Let $\mathrm{d}\mu = r(x)^\alpha \mathrm{d}x$; this defines a measure for all $\alpha \in \mathbb{R}$, and the triple $(\Omega, \sigma, \mathrm{d}\mu)$ constitutes a measure space. The space $L^2_\alpha(\Omega)$ can then equivalently be defined as the L^2 space on $(\Omega, \sigma, \mathrm{d}\mu)$:

$$L^2(\Omega; \mathrm{d}\mu) = \{u \text{ measurable } : \int_\Omega u^2 \mathrm{d}\mu < \infty\}.$$

Thus, $L^2_\alpha(\Omega)$ admits the standard properties of L^2 spaces with respect to $(\Omega, \sigma, \mathrm{d}\mu)$, such as density of smooth functions $C^\infty_0(\Omega; \mathrm{d}\mu)$. In particular, it is complete [40, Theorem 13.11].

Let $H^m_\alpha(\Omega)$ denote the space [35, 33]:

$$H^m_\alpha(\Omega) = \{u \in L^2_\alpha(\Omega) : D^\beta u \in L^2_\alpha(\Omega) \text{ for all } |\beta| \leq m\}.$$

This is a Hilbert space equipped with the inner product

$$(u, v)_{H^m_\alpha(\Omega)} = \sum_{|\beta| \leq m} (D^\beta u, D^\beta v)_{L^2_\alpha(\Omega)}$$

and is a Sobolev space in the sense that $r^\alpha u \in H^m(\Omega)$. The space $H^m_\alpha(\Omega)$ is often referred to as a nonhomogeneous weighted Sobolev space, as the weight is not adjusted to compensate for the regularity lost when taking a derivative. In this work, we shall work mainly with homogeneous weighted Sobolev spaces of the type [33, 29, 26]

$$V^m_\alpha(\Omega) = \{u \in L^2_{\alpha-1}(\Omega) : D^\beta u \in L^2_{\alpha+|\beta|-m}(\Omega) \text{ for all } |\beta| \leq m\},$$

which is a Hilbert space with the inner product

$$(u,v)_{V^m_\alpha(\Omega)} = \sum_{|\beta|\leq m} (D^\beta u, D^\beta v)_{L^2_{\alpha+|\beta|-m}(\Omega)}.$$

For $m=1$, we then have $V^1_\alpha(\Omega) = \{u \in L^2_{\alpha-1}(\Omega) : \nabla u \in (L^2_\alpha(\Omega))^3\}$. The $H^m_\alpha(\Omega)$ and $V^m_\alpha(\Omega)$ norms are equivalent; this follows from the following inequality [6, Theorem 2.1]:

$$\|u\|_{L^2_{\alpha-1}(\Omega)} \leq C_\alpha \|u\|_{H^1_\alpha(\Omega)}. \tag{2.2}$$

The properties of the spaces $H^1_\alpha(\Omega)$ and $V^1_\alpha(\Omega)$ depend on the choice of weights. For $\alpha \in (-1,1)$, the weights used in the space $H^1_\alpha(\Omega)$ are both Muckenhoupt. One then has density of smooth functions and the imbedding $L^1(\Omega) \subset H^1_\alpha(\Omega)$. By equivalence of norms, the same holds for the space $V_\alpha(\Omega)$.

Finally, let us define the weighted H-div–type space $V_{\alpha+1}(\mathrm{div};\Omega)$:

$$V_{\alpha+1}(\mathrm{div};\Omega) = \{\mathbf{q} \in (L^2_\alpha(\Omega))^3 : \nabla\cdot\mathbf{q} \in L^2_{\alpha+1}(\Omega)\}.$$

This is a Hilbert space equipped with the inner product

$$(\mathbf{q},\mathbf{v})_{V_{\alpha+1}(\Omega;\mathrm{div})} = (\mathbf{q},\mathbf{v})_{L^2_\alpha(\Omega)} + (\nabla\cdot\mathbf{q}, \nabla\cdot\mathbf{v})_{L^2_{\alpha+1}(\Omega)}.$$

Note that elements of this space have a weak divergence $\nabla\cdot\mathbf{q} \in L^2_{\alpha+1}(\Omega)$, which is non-Muckenhoupt for $\alpha > 0$. Consequently, the weak divergence of functions in $V_{\alpha+1}(\mathrm{div};\Omega)$ may not belong to $L^1(\Omega)$.

3. Existence of a solution. In the previous section, we gave the definition of the weighted Sobolev spaces. With these at our disposal, we are now ready to give the variational formulation of (1.1a)–(1.1c): Find $(u,\mathbf{q}) \in L^2_{\alpha-1}(\Omega) \times V_{\alpha+1}(\mathrm{div};\Omega)$ such that

$$(\kappa^{-1}\mathbf{q},\mathbf{v}) - (u, \nabla\cdot\mathbf{v}) + (u_0, \mathbf{v}\cdot\mathbf{n})_{\partial\Omega} = 0 \qquad \forall\, \mathbf{v} \in V_{-\alpha+1}(\mathrm{div};\Omega), \tag{3.1a}$$

$$(\nabla\cdot\mathbf{q},\theta) = (f\tilde{\delta}_\Lambda, \theta) \qquad \forall\, \theta \in L^2_{-\alpha-1}(\Omega), \tag{3.1b}$$

where $\mathbf{n}$ is the unit normal of $\partial\Omega$ and $\tilde{\delta}_\Lambda$ is defined as

$$\tilde{\delta}_\Lambda = \lim_{\epsilon\to 0} \delta^\epsilon_\Lambda \text{ in } L^2_{\alpha+1}(\Omega), \tag{3.2}$$

with δ^ϵ_Λ being the sequence of nascent Dirac functions defined in (1.3). We note that it is necessary here to interpret the Dirac line source in a weighted rather than distributional sense, as the test function $\theta \in L^2_{-\alpha-1}(\Omega)$ may not be smooth enough to admit a trace on Λ. To be more precise, the limit $(f\delta_\Lambda,\theta) = \lim_{\epsilon\to 0}(f,\theta)_{\Omega_\epsilon} = (f,\theta)_\Lambda$ may not be well defined. For the variational formulation (3.1a)–(3.1b), we therefore interpret the line source in the sense of weighted L^2 spaces and show that $\tilde{\delta}_\Lambda \in L^2_{\alpha+1}(\Omega)$.

The solution space is chosen so that $r^{\alpha-1}u \in L^2(\Omega)$, $r^\alpha\mathbf{q} \in (L^2(\Omega)^3)$, and $r^{\alpha+1}\nabla\cdot\mathbf{q} \in L^2(\Omega)$, where the weighing is increased to account for the regularity loss caused by taking a derivative. This ensures that the velocity and pressure spaces are sufficiently large to capture the expected structure of the solution while selecting the largest test spaces admissible with respect to the bilinear forms appearing in the variational formulation. The main result of this section is the following existence theorem.

THEOREM 3.1. *Let $\Omega \subset \mathbb{R}^3$ be a bounded open 3D domain with smooth boundary $\partial\Omega$, $\Lambda \subset \Omega$ be a differentiable manifold with topological dimension 1, $u_0 \in C^2(\bar{\Omega})$, $f \in C^0(\bar{\Omega})$, and $\kappa \in L^\infty(\Omega)$ be strictly positive. For $\alpha > 0$ small enough, there then exists $(u, \mathbf{q}) \in L^2_{\alpha-1}(\Omega) \times V_{\alpha+1}(\mathrm{div}; \Omega)$ solving* (3.1a)–(3.1b).

The proof of Theorem 3.1 relies on two lemmas. The first of these guarantees a solution to (3.1a)–(3.1b) for a source term $g \in L^2_{\alpha+1}(\Omega)$ for $\alpha > 0$ small enough.

LEMMA 3.2. *Let $g \in L^2_{\alpha+1}(\Omega)$ with $\alpha > 0$ small enough. Under the assumptions of Theorem* 3.1*, there then exists $(u, \mathbf{q}) \in L^2_{\alpha-1}(\Omega) \times V_{\alpha+1}(\mathrm{div}; \Omega)$ solving*

$$(\kappa^{-1}\mathbf{q}, \mathbf{v}) - (\nabla \cdot \mathbf{v}, u) + (u_0, \mathbf{v} \cdot \mathbf{n})_{\partial\Omega} = 0 \qquad \forall\, \mathbf{v} \in V_{-\alpha+1}(\mathrm{div}; \Omega), \tag{3.3a}$$

$$(\nabla \cdot \mathbf{q}, \theta) = (g, \theta) \qquad \forall\, \theta \in L^2_{-\alpha-1}(\Omega). \tag{3.3b}$$

The second lemma addresses the line source interpreted in the sense of (3.2).

LEMMA 3.3. *For $\alpha > 0$ and $\tilde{\delta}_\Lambda$ in* (1.3)*, one has $\tilde{\delta}_\Lambda \in L^2_{\alpha+1}(\Omega)$.*

This section will proceed as follows. First, we state the Brezzi–Nečas–Babuška (BNB) theorem [8, Theorem 2.1] (sometimes referred to as the generalized Lax–Milgram theorem). After this, we give a proof of Lemma 3.2; this is done by verifying the assumptions of the BNB theorem. Next, we give a proof of Lemma 3.3. This is done by showing that the sequence δ^ϵ_Λ is Cauchy in $L^2_{\alpha+1}(\Omega)$ (which is complete) and thus converges in $L^2_{\alpha+1}(\Omega)$. It follows that the line source $\tilde{\delta}_\Lambda$ belongs to $L^2_{\alpha+1}(\Omega)$. We conclude by giving a proof of Theorem 3.1.

THEOREM 3.4 (BNB theorem). *Let X_i and M_i be real reflexive Banach spaces $(i = 1, 2)$. Assume we are given three continuous bilinear forms: $a : X_2 \times X_1 \to \mathbb{R}$, $b_1 : X_1 \times M_1 \to \mathbb{R}$, $b_2 : X_2 \times M_2 \to \mathbb{R}$. For any given $g_1 \in (X_1)^*$ and $g_2 \in (M_2)^*$, we consider the following problem:*

Find $(q, u) \in X_2 \times M_1$ s.t.

$$a(q, v) + b_1(v, u) = \langle g_1, v \rangle, \tag{3.4a}$$

$$b_2(q, \theta) = \langle g_2, \theta \rangle \tag{3.4b}$$

for all $(v, \theta) \in X_1 \times M_2$.

Let K_i denote the kernel space of b_i:

$$K_i = \{v \in X_i : b_i(v, u) = 0 \quad \forall\, u \in M_i\}.$$

The problem (3.4a)–(3.4b) *then admits a solution $(\mathbf{q}, u) \in X_2 \times M_1$ if the following assumptions hold:*

Condition (C_0): Weak coercivity of $a(\cdot, \cdot)$: There exists constants $\gamma_1, \gamma_2 > 0$ s.t.

$$\sup_{v \in K_1} \frac{a(q, v)}{\|v\|_{X_1}} \geq \gamma_1 \|q\|_{X_2} \quad \forall\, q \in K_2 \tag{3.5}$$

and

$$\sup_{q \in K_2} \frac{a(q, v)}{\|q\|_{X_2}} \geq \gamma_2 \|v\|_{X_1} \quad \forall\, v \in K_1. \tag{3.6}$$

Condition (C_i): Inf-sup condition on $b_i(\cdot, \cdot)$: For $i = 1, 2$, there exists $\beta_i > 0$ s.t.

$$\sup_{v \in X_i} \frac{b_i(v, u)}{\|v\|_{X_i}} \geq \beta_i \|u\|_{M_i} \quad \forall\, u \in M_i. \tag{3.7}$$

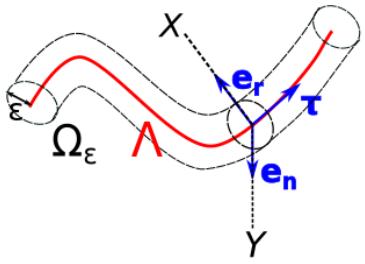

FIG. 3.1. *A generalized cylinder Ω_ϵ with centerline Λ and a constant radius ϵ. The curve Λ is associated with a Frenet frame $\mathbf{e}_r, \mathbf{e}_n, \boldsymbol{\tau}$; here, $\boldsymbol{\tau}$ denotes its unit tangent vector, $\mathbf{e}_r$ its unit normal vector, and $\mathbf{e}_n$ its unit binormal vector.*

Proof of Lemma 3.2. The proof consists of verifying the conditions of the BNB theorem, taking the variational forms

$$\begin{aligned} a(\mathbf{q},\mathbf{v}) &= (\kappa^{-1}\mathbf{q},\mathbf{v}),\\ b_1(\mathbf{q},\theta) = b_2(\mathbf{q},\theta) := b(\mathbf{q},\theta) &= -(\nabla\cdot\mathbf{q},\theta),\\ \langle g_1, v\rangle &= -(u_0,\mathbf{v}\cdot\mathbf{n})_{\partial\Omega},\\ \langle g_2,\theta\rangle &= (g,\theta) \end{aligned}$$

and the function spaces $X_2 = V_{\alpha+1}(\mathrm{div};\Omega)$, $X_1 = V_{-\alpha+1}(\mathrm{div};\Omega)$, $M_1 = L^2_{\alpha-1}(\Omega)$, and $M_2 = L^2_{-\alpha-1}(\Omega)$. The kernel spaces K_1 and K_2 are then given as

$$\begin{aligned} K_1 &= \{\mathbf{v}\in V_{-\alpha+1}(\mathrm{div};\Omega) : b_1(\mathbf{v},u) = 0 \quad \forall\, u\in L^2_{\alpha-1}(\Omega)\},\\ K_2 &= \{\mathbf{q}\in V_{\alpha+1}(\mathrm{div};\Omega) : b_2(\mathbf{q},\theta) = 0 \quad \forall\,\theta\in L^2_{-\alpha-1}(\Omega)\}. \end{aligned}$$

By an application of Cauchy–Schwarz (2.1), it follows that the bilinear form $a(\cdot,\cdot)$ is bounded on $V_{\alpha+1}(\mathrm{div};\Omega)\times V_{-\alpha+1}(\mathrm{div};\Omega)$. The same holds true for $b_2(\cdot,\cdot)$ on $V_{\alpha+1}(\mathrm{div};\Omega)\times L^2_{-\alpha-1}(\Omega)$ and $b_1(\cdot,\cdot)$ on $V_{-\alpha+1}(\mathrm{div};\Omega)\times L^2_{\alpha-1}(\Omega)$. Next, as the dual space of $L^2_{\alpha+1}(\Omega)$ coincides with $L^2_{-\alpha-1}(\Omega)$, the duality pairing $\langle g_2,\theta\rangle$ is well defined with $g_2 = g$. Finally, the boundedness of the form $(u_0,\mathbf{v}\cdot\mathbf{n})_{\partial\Omega}$ follows from standard theory, as the weighted Sobolev spaces are equivalent with standard spaces away from Λ.

Before we show (3.5) in Condition (C_0), let us first note a central property of the kernel spaces K_1 and K_2. Fix arbitrary $\mathbf{q}\in K_2$, and take $\theta = r^{2(\alpha+1)}\nabla\cdot\mathbf{q}\in L^2_{-\alpha-1}(\Omega)$. This yields $b(\mathbf{q}, r^{2(\alpha+1)}\nabla\cdot\mathbf{q}) = \|\nabla\cdot\mathbf{q}\|_{L^2_{\alpha+1}(\Omega)} = 0$ for all $\mathbf{q}\in K_2$. Switching $\mathbf{q}$ with $\mathbf{v}$ and reversing the sign of α, one similarly finds $\|\nabla\cdot\mathbf{v}\|_{L^2_{-\alpha+1}(\Omega)} = 0$ for all $\mathbf{v}\in K_1$.

We now show (3.5). Fixing again $\mathbf{q}\in K_2$, the proof is by construction of a suitable $\mathbf{v}_\mathbf{q}\in K_1$. We begin by giving this construction. Let $\mathbf{v}_\mathbf{q} = r^{2\alpha}\mathbf{q} + \boldsymbol{\Psi}$, where $\boldsymbol{\Psi}$ is the solution of $\nabla\cdot\boldsymbol{\Psi} = -2\alpha r^{2\alpha-1}\nabla r\cdot\mathbf{q}$. To see that such a suitable function $\boldsymbol{\Psi}$ exists, set $\boldsymbol{\Psi} = -\nabla\phi$; one then has $-\Delta\phi = -2\alpha r^{2\alpha-1}\nabla r\cdot\mathbf{q} := f_\phi$. Note that $\nabla r = \mathbf{e}_r$, where $\mathbf{e}_r$ denotes the unit normal with respect to Λ, as illustrated in Figure 3.1. A calculation then shows $f_\phi\in L^2_{-\alpha+1}(\Omega)$. By [39, Theorem 1.2.8], there then exists $\phi\in V^2_{-\alpha+1}(\Omega)$ satisfying

$$\|\phi\|_{V^2_{-\alpha+1}(\Omega)} \le C_S\|f_\phi\|_{L^2_{-\alpha+1}(\Omega)} \le 2|\alpha|C_S\|\mathbf{q}\|_{L^2_\alpha(\Omega)}, \tag{3.8}$$

where $C_S > 0$ denotes some stability constant. With this in hand, we can verify $\mathbf{v}_\mathbf{q}\in V_{-\alpha+1}(\mathrm{div};\Omega)$. First, $\|\boldsymbol{\Psi}\|_{V_{-\alpha+1}(\mathrm{div};\Omega)} \le \|\phi\|_{V^2_{-\alpha+1}(\Omega)}$. Combining this with

(3.8), one then has $\Psi \in V_{-\alpha+1}(\mathrm{div};\Omega)$. Similarly, we have $r^{2\alpha}\mathbf{q} \in V_{-\alpha+1}(\mathrm{div};\Omega)$; to see this, we calculate

$$\begin{aligned}\|r^{2\alpha}\mathbf{q}\|^2_{V_{-\alpha+1}(\mathrm{div};\Omega)} &= \|r^{2\alpha}\mathbf{q}\|^2_{L_{-\alpha}(\Omega)} + \|\nabla\cdot(r^{2\alpha}\mathbf{q})\|^2_{L_{-\alpha+1}(\Omega)}\\ &\le \|\mathbf{q}\|^2_{L_\alpha(\Omega)} + \|r^{2\alpha}\nabla\cdot\mathbf{q}\|^2_{L_{-\alpha+1}(\Omega)} + \|2\alpha r^{2\alpha-1}\mathbf{e}_r\cdot\mathbf{q}\|^2_{L_{-\alpha+1}(\Omega)}\\ &= \|\mathbf{q}\|^2_{L_\alpha(\Omega)} + \|\nabla\cdot\mathbf{q}\|^2_{L_{\alpha+1}(\Omega)} + \|2\alpha\mathbf{e}_r\cdot\mathbf{q}\|^2_{L_\alpha(\Omega)}\\ &\le (1+2|\alpha|)\|\mathbf{q}\|^2_{V_{\alpha+1}(\mathrm{div};\Omega)}.\end{aligned}$$

It follows that $\mathbf{v_q} \in V_{-\alpha+1}(\mathrm{div};\Omega)$. Finally, we can verify $\mathbf{v_q} \in K_1$. By the product rule, one has $\nabla\cdot\mathbf{v_q} = r^{2\alpha}\nabla\cdot\mathbf{q}$. For $u \in L^2_{\alpha-1}$, it follows that

$$b(\mathbf{v_q},u) = (\nabla\cdot\mathbf{v_q},u) = (\nabla\cdot\mathbf{q}, r^{2\alpha}u) = 0 \tag{3.9}$$

as $r^{2\alpha}u \in L^2_{-\alpha-1}$ and $\mathbf{q} \in K_2$.

With the construction $\mathbf{v} = r^{2\alpha}\mathbf{q} + \mathbf{\Psi} \in K_1$ in hand, one can finally proceed to show (3.5). First,

$$\begin{aligned}a(\mathbf{q},\mathbf{v_q}) &= a(\mathbf{q}, r^{2\alpha}\mathbf{q}) + a(\mathbf{q},\mathbf{\Psi}) = \|\kappa^{-\frac{1}{2}}\mathbf{q}\|^2_{L^2_\alpha(\Omega)} + a(\mathbf{q},\mathbf{\Psi})\\ &\ge \|\kappa^{-\frac{1}{2}}\mathbf{q}\|^2_{L^2_\alpha(\Omega)} - |a(\mathbf{q},\mathbf{\Psi})|\\ &\ge \frac{1}{C_{\kappa,\max}}\|\mathbf{q}\|^2_{L^2_\alpha(\Omega)} - \frac{1}{C_{\kappa,\min}}\|\mathbf{q}\|_{L^2_\alpha(\Omega)}\|\mathbf{\Psi}\|_{L^2_{-\alpha}(\Omega)}\\ &\ge \frac{1}{C_{\kappa,\max}}\|\mathbf{q}\|^2_{L^2_\alpha(\Omega)} - \frac{1}{C_{\kappa,\min}}\|\mathbf{q}\|_{L^2_\alpha(\Omega)}\|\mathbf{\Psi}\|_{V^1_{-\alpha+1}(\Omega)}\\ &\ge \left(\frac{1}{C_{\kappa,\max}} - \frac{1}{C_{\kappa,\min}}2|\alpha|C_S\right)\|\mathbf{q}\|^2_{L^2_\alpha(\Omega)},\end{aligned} \tag{3.10}$$

where $C_{\kappa,\min}, C_{\kappa,\max}$ are constants associated with κ. Next, $\|\nabla\cdot\mathbf{q}\|_{L^2_{\alpha+1}(\Omega)} = 0$, meaning that

$$a(\mathbf{q},\mathbf{v_q}) \ge \left(\frac{1}{C_{\kappa,\max}} - \frac{1}{C_{\kappa,\min}}2|\alpha|C_S\right)\|\mathbf{q}\|^2_{V^1_{\alpha+1}(\Omega)}. \tag{3.11}$$

A further computation shows

$$\begin{aligned}\|\mathbf{v_q}\|^2_{V_{-\alpha+1}(\mathrm{div};\Omega)} &\le \|r^{2\alpha}\mathbf{q}\|^2_{L^2_{-\alpha}(\Omega)} + \|\mathbf{\Psi}\|^2_{L^2_{-\alpha}(\Omega)} + \|r^{2\alpha}\nabla\cdot\mathbf{q}\|^2_{L^2_{-\alpha+1}(\Omega)}\\ &\le (1+2|\alpha|C_S)\|\mathbf{q}\|^2_{L^2_\alpha(\Omega)} + \|\nabla\cdot\mathbf{q}\|^2_{L^2_{\alpha+1}(\Omega)}\\ &\le (1+2|\alpha|C_S)\|\mathbf{q}\|^2_{V_{\alpha+1}(\mathrm{div};\Omega)}.\end{aligned} \tag{3.12}$$

Combining (3.11) and (3.12), it follows that

$$\begin{aligned}\sup_{\mathbf{v}\in K_1}\frac{a(\mathbf{q},\mathbf{v})}{\|\mathbf{v}\|_{V_{-\alpha+1}(\mathrm{div};\Omega)}} &\ge \frac{a(\mathbf{q},\mathbf{v_q})}{\|\mathbf{v_q}\|_{V_{-\alpha+1}(\mathrm{div};\Omega)}}\\ &\ge \frac{\left(\frac{1}{C_{\kappa,\max}} - \frac{1}{C_{\kappa,\min}}2|\alpha|C_S\right)}{\sqrt{1+2|\alpha|C_S}}\|\mathbf{q}\|_{V_{\alpha+1}(\mathrm{div};\Omega)} \quad \forall\,\mathbf{q}\in K_2,\end{aligned} \tag{3.13}$$

where the right-hand side is positive given

$$|\alpha| < \frac{1}{2}\frac{C_{\kappa,\min}}{C_{\kappa,\max}C_S}. \tag{3.14}$$

For α small enough, (3.5) then holds for some $\gamma_1 > 0$. To show that (3.6) holds, one can switch the sign of α and repeat this argument with $(\theta, \mathbf{q}_\mathbf{v})$ switched with $(u, \mathbf{v}_\mathbf{q})$. It follows that Condition (C_0) holds.

Next we will verify Condition (C_i). Consider first $i = 1$. For a given $u \in L^2_{\alpha-1}(\Omega)$, we now define $\mathbf{v}_u$ as the solution of the equation $\nabla \cdot \mathbf{v}_u = r^{2\alpha-2}u \in L^2_{1-\alpha}(\Omega)$. Setting $\mathbf{v}_u = -\nabla\xi$ then requires solving the Poisson problem $-\Delta\xi = r^{2\alpha-2}u$, where $r^{2\alpha-2}u \in L^2_{\alpha-1}$. Invoking again [39, Theorem 1.2.8], we know there exists such a solution $\xi \in V^2_{\alpha-1}(\Omega)$ such that $\|\xi\|_{V^2_{\alpha+1}(\Omega)} \leq C_S\|u\|_{L^2_{\alpha-1}(\Omega)}$, where C_S denotes a stability constant. Thus, a solution $\mathbf{v}_u \in V_{\alpha-1}(\mathrm{div};\Omega)$ exists solving $\nabla \cdot \mathbf{v}_u = r^{2\alpha-2}u$ such that $\|\mathbf{v}_u\|_{V_{-\alpha+1}(\mathrm{div};\Omega)} \leq C_S\|u\|_{L^2_{\alpha-1}\Omega}$. For this $\mathbf{v}_u$, $b(\mathbf{v}_u, u) = (r^{\alpha-1}u, r^{\alpha-1}u)) = \|u\|^2_{L^2_{\alpha-1}(\Omega)}$. It follows that

$$\sup_{\mathbf{v}\in X_1}\frac{b_1(\mathbf{v},u)}{\|\mathbf{v}\|_{X_1}} \geq \frac{b_1(\mathbf{v}_u,u)}{\|\mathbf{v}_u\|_{V_{-\alpha+1}(\mathrm{div};\Omega)}} = \frac{\|u\|^2_{L^2_{\alpha-1}}}{\|\mathbf{v}_u\|_{V_{-\alpha+1}(\mathrm{div};\Omega)}} \geq \beta_1\|u\|_{L^2_{\alpha-1}(\Omega)},$$

and (3.7) holds with $\beta_1 = 1/C_S$. To show (3.7) for $i = 2$, one can switch the sign of α and repeat this argument with $(\theta, \mathbf{q}_\theta)$ switched with $(u, \mathbf{v}_u)$. ∎

Proof of Lemma 3.3. First, let us rewrite $\tilde{\delta}_\Lambda$ to an equivalent definition using $\epsilon = 1/k$,

$$\tilde{\delta}_\Lambda = \lim_{k\to\infty}\delta^k_\Lambda, \quad \delta^k_\Lambda = \begin{cases} \frac{k^2}{\pi} & \text{for } \mathbf{x} \in \Omega_{1/k}, \\ 0 & \text{otherwise,} \end{cases} \tag{3.15}$$

where the limit is taken in $L^2_{\alpha+1}(\Omega)$. The proof is by showing that δ^k_Λ is a Cauchy sequence in $L^2_{\alpha+1}(\Omega)$ for $\alpha > 0$.

For each $k \in \mathbb{R}$, the function δ^k_Λ can be interpreted as the indicator function of a generalized cylinder $\Omega_{1/k}$ with centerline Λ and a constant radius $1/k$. Using then the notation of generalized cylinders [19], we let $\mathbf{e}_r, \mathbf{e}_n, \boldsymbol{\tau}$ be the Frenet frame of Λ, as illustrated in Figure 3.1. We further let X and Y denote the axes along the vectors $\mathbf{e}_r, \mathbf{e}_n$ of the Frenet frame; the coordinate axes X, Y thus form a local coordinate system having origin on Λ. With this notation in hand, we have

$$\begin{aligned}
\|\delta^{k+m}_\Lambda - \delta^k_\Lambda\|^2_{L^2_{\alpha+1}(\Omega)} &= \int_{\Omega_{1/k}}(\delta^{k+m}_\Lambda - \delta^k_\Lambda)^2 r^{2\alpha+2}\mathrm{d}\omega \\
&= \int_\Lambda\int_{D(s)}(\delta^{k+m}_\Lambda - \delta^k_\Lambda)^2 r^{2\alpha+2}\mathrm{d}X(s)\mathrm{d}Y(s)\mathrm{d}s \\
&= \int_0^L \|\boldsymbol{\lambda}'(s)\| \underbrace{\int_0^{2\pi}\int_0^{\frac{1}{k}}(\delta^{k+m}_\Lambda - \delta^k_\Lambda)^2 r^{2\alpha+2} r\mathrm{d}r(s)\mathrm{d}\theta(s)}_{I(r,\theta;s)}\mathrm{d}s,
\end{aligned}$$

where ω denotes the generic volume Lebesgue measure, $\|\boldsymbol{\lambda}'(s)\|$ the Jacobian of $\boldsymbol{\lambda}$, $\|\cdot\|$ the Euclidean norm, $D(s)$ some parametrization of the cross section of $\Omega_{1/k}$ at the point $\boldsymbol{\lambda}(s)$, L the length of Λ, and $r(s), \theta(s)$ the polar coordinates of X, Y.

Consider for a moment s to be fixed. A calculation then shows

$$\begin{aligned} I(r,\theta;s) &= \int_0^{2\pi}\int_0^{\frac{1}{k}} (\delta_\Lambda^{k+m}-\delta_\Lambda^k)^2 r^{2\alpha+2} r\mathrm{d}r\mathrm{d}\theta \\ &= \frac{2\pi}{\pi^2}\left(\int_0^{\frac{1}{k+m}} ((k+m)^2-k^2)^2 r^{2\alpha+3}\mathrm{d}r + \int_{\frac{1}{k+m}}^{\frac{1}{k}} k^4 r^{2\alpha+3}\mathrm{d}r\right) \\ &= \frac{2}{\pi(2\alpha+4)}\left(k^{-2\alpha}+(m^2(2k+m)^2-k^4)(k+m)^{-4-2\alpha}\right). \end{aligned}$$

Note now that each term in the last line has a negative exponent, meaning that each term has a zero limit as $k,m\to\infty$. It follows that

$$\lim_{k,m\to\infty} I(r,\theta;s)=0, \tag{3.16}$$

and consequently

$$\lim_{k,m\to\infty} \|\delta_\Lambda^{k+m}-\delta_\Lambda^k\|^2_{L^2_{\alpha+1}(\Omega)}=0. \tag{3.17}$$

The sequence is thus Cauchy. Moreover, as the space $L^2_{\alpha+1}(\Omega)$ is complete, it follows that

$$\lim_{k\to\infty}\delta_\Lambda^k=\tilde{\delta}_\Lambda\in L^2_{\alpha+1}(\Omega). \tag{3.18}$$ ∎

Finally, with Lemmas 3.2 and 3.3 in hand, the proof of Theorem 3.1 is straightforward.

Proof of Theorem 3.1. By Lemma 3.3, one has $\tilde{\delta}_\Lambda$ belonging to $L^2_{\alpha+1}(\Omega)$. Consequently, one has by Cauchy–Schwarz

$$(f\tilde{\delta}_\Lambda,\theta)_\Omega\le\|f\|_{L^\infty(\Omega)}\|\tilde{\delta}_\Lambda\|_{L^2_{\alpha+1}(\Omega)}\|\theta\|_{L^2_{-\alpha-1}(\Omega)}. \tag{3.19}$$

By Lemma 3.2, the problem (3.1a)–(3.1b) then satisfies all the conditions of the BNB theorem. ∎

4. Solution splitting. In the previous section, we proved the existence of $(u,\mathbf{q})\in L^2_{\alpha-1}(\Omega)\times V_{\alpha+1}(\mathrm{div};\Omega)$ solving (3.1a)–(3.1b). As was discussed in section 2, the space $V_{\alpha+1}(\mathrm{div};\Omega)$ is not Muckenhoupt. Consequently, $V_{\alpha+1}(\mathrm{div};\Omega)\not\subset L^1(\Omega)$. This leaves the approximation properties of $V_{\alpha+1}(\mathrm{div};\Omega)$ nonstandard.

In this section, we will construct a solution splitting that can later be used to define a singularity removal–based method for approximating $(u,\mathbf{q})$. Let Λ be a straight line segment $\Lambda\subset\Omega$ and $f\in C^2(\bar{\Omega})$ and $\kappa\in W^{2,\infty}(\Omega)$ be scalar valued such that $\kappa>0$. To make the derivations simpler to follow, we further assume that κ is constant and that $f=f(s)$ in Ω_ϵ for some $\epsilon>0$. The first of these assumptions could be dropped using the splitting shown in [21, section 3.3]. The second assumption can be dropped by the use of an extension operator; this is discussed in Remark 3.

With the stated assumptions in hand, consider again the strong formulation of the line source problem:

$$\begin{aligned} \mathbf{q}+\kappa\nabla u &= 0 && \text{in } \Omega, \\ \nabla\cdot\mathbf{q} &= f\delta_\Lambda && \text{in } \Omega, \\ u &= u_0 && \text{on } \partial\Omega. \end{aligned}$$

The solution then admits a splitting into higher- and lower-regularity terms

$$(u, \mathbf{q}) = (u_s, \mathbf{q}_s) + (u_r, \mathbf{q}_r) \text{ where } \begin{cases} (u_s, \mathbf{q}_s) & \in L^2_{\alpha-1}(\Omega) \times V_{\alpha+1}(\mathrm{div}; \Omega), \\ (u_r, \mathbf{q}_r) & \in L^2(\Omega) \times H(\mathrm{div}; \Omega). \end{cases} \tag{4.1}$$

Here, the lower-regularity pair $(u_s, \mathbf{q}_s)$ is defined as

$$u_s := fG, \quad \mathbf{q}_s := -\kappa \nabla u_s, \tag{4.2}$$

with G taken as the solution of

$$-\kappa \Delta G = \delta_\Lambda \quad \text{in } \mathbb{R}^3 \tag{4.3}$$

in an appropriately weak sense. In the next section, we will show that this property ensures that $(u_s, \mathbf{q}_s)$ capture the singular behavior by δ_Λ. This allows the remainder pair $(u_r, \mathbf{q}_r)$ to enjoy higher regularity. Inserting (4.1) into (1.1a)–(1.1c) and using (4.3), one finds that the remainder pair must satisfy

$$\mathbf{q}_r + \kappa \nabla u_r = 0 \qquad \text{in } \Omega, \tag{4.4a}$$

$$\nabla \cdot \mathbf{q}_r = f_r \qquad \text{in } \Omega, \tag{4.4b}$$

$$u_r = u_{r,0} \qquad \text{on } \partial\Omega, \tag{4.4c}$$

with

$$f_r = \kappa \left(\Delta f \, G + 2 \nabla f \cdot \nabla G \right), \tag{4.5a}$$

$$u_{r,0} = u_0 - fG. \tag{4.5b}$$

Thus, (1.1a)–(1.1c) can be solved by finding $(u_r, \mathbf{q}_r)$ satisfying (4.4a)–(4.4c) and reconstructing $(u, \mathbf{q})$ from (4.1). As $(u_r, \mathbf{q}_r)$ enjoy higher regularity compared to the full solution, one expects this approach to yield improved approximation properties. We will return to this observation in section 5 when introducing a numerical approach to approximate the solution.

The section will proceed as follows. In section 4.1, we show how one can construct the solution splitting (4.1) so that $(u_s, \mathbf{q}_s)$ capture the solution singularity. In section 4.2, we discuss in more detail the regularity of the splitting terms. In particular, we give a justification of (4.1).

4.1. Construction of the solution splitting. In this section, we will show how to construct the solution splitting in (4.1). The solution splitting can be constructed in two steps: (1) identifying an explicit function G capturing the solution singularity induced by δ_Λ and (2) identifying the system that the remainder pair $(u_r, \mathbf{q}_r)$ must solve.

Let us start with the first step. Let $\mathcal{L} = -\kappa\Delta$ denote the differential operator in (1.1a)–(1.1b). Formally, $\mathcal{L}G$ should return the "unit line source," meaning that $\mathcal{L}G = \delta_\Lambda$ in the sense of distributions. Let G_{3D} denote Green's function of $\mathcal{L}$ in $\mathbb{R}^3$,

$$G_{3D}(\mathbf{x}) = \frac{1}{4\pi\kappa} \frac{1}{\|\mathbf{x}\|}, \tag{4.6}$$

where $\|\cdot\|$ denotes the Euclidean norm. By the theory of Green's functions, a candidate G can then be defined as $G = \delta_\Lambda * G_{3D}$, where $*$ denotes the convolution operator.

By the definition of the Dirac line source in (1.3), we have

$$\begin{aligned} G(\mathbf{x}) &= \lim_{\epsilon\to 0}\int_\Omega \delta_\Lambda^\epsilon(\mathbf{y}) G_{3D}(\mathbf{x}-\mathbf{y})\,\mathrm{d}\mathbf{y} \\ &= \lim_{\epsilon\to 0}\int_{\Omega_\epsilon} \frac{1}{\pi\epsilon^2} G_{3D}(\mathbf{x}-\mathbf{y})\,\mathrm{d}\mathbf{y}. \end{aligned} \tag{4.7}$$

Let now $\mathbf{x}\in\Omega$ be such that $\mathbf{x}\not\in\Lambda$. For any $\mathbf{y}\in\Omega_\epsilon$ and ϵ small enough, one then has $\mathbf{x}-\mathbf{y}\not\in\Omega_\epsilon$ for all $\mathbf{y}\in\Omega_\epsilon$. Thus, $G_{3D}(\mathbf{x}-\mathbf{y})$ is continuous in the integration domain Ω_ϵ. Invoking the mean-value theorem, one has

$$\begin{aligned} G(\mathbf{x}) &= \int_\Lambda \lim_{\epsilon\to 0}\int_{D(s)} \frac{1}{\pi\epsilon^2} G_{3D}(\mathbf{x}-\mathbf{y})\,\mathrm{d}\mathbf{y} \\ &= \int_\Lambda \lim_{\epsilon\to 0} \frac{\pi\epsilon^2}{\pi\epsilon^2} G_{3D}(\mathbf{x}-\mathbf{c})\,\mathrm{d}s, \end{aligned}$$

where $\mathbf{c}\in D(s)$ and $D(s)$ again denote the same parametrization of the cross section of Ω_ϵ at $\boldsymbol{\lambda}(s)$. Passing to the limit, one then has

$$G(\mathbf{x}) = \int_\Lambda G_{3D}(\mathbf{x}-\boldsymbol{\lambda}(s))\,\mathrm{d}s. \tag{4.8}$$

An explicit solution for G can thus be found by evaluating this line integral. To do so, note that the line segment Λ can be described by the parametrization $\Lambda : \mathbf{a}+\boldsymbol{\tau}s$ for $s\in(0,L)$, where $\boldsymbol{\tau}$ denotes the normalized tangent vector of Λ, i.e., $\boldsymbol{\tau}=(\mathbf{b}-\mathbf{a})/L$. A calculation then reveals

$$\begin{aligned} G(\mathbf{x}) &= \frac{1}{4\pi}\int_\Lambda \frac{1}{\|\mathbf{x}-\boldsymbol{\lambda}(s)\|}\,\mathrm{d}s \\ &= \frac{1}{4\pi}\int_0^L \frac{1}{\|\mathbf{x}-(\mathbf{a}+\boldsymbol{\tau}s)\|}\,\mathrm{d}s \\ &= \frac{1}{4\pi}\ln\left(\frac{r_b+L+\boldsymbol{\tau}\cdot(\mathbf{a}-\mathbf{x})}{r_a+\boldsymbol{\tau}\cdot(\mathbf{a}-\mathbf{x})}\right), \end{aligned} \tag{4.9}$$

where $r_a=\|\mathbf{x}-\mathbf{a}\|$ and $r_b=\|\mathbf{x}-\mathbf{b}\|$.

Returning to the splitting ansatz $(u,\mathbf{q})=(u_s,\mathbf{q}_s)+(u_r,\mathbf{q}_r)$, the singular solution pair can then be defined as in (4.1). Inserting (4.1) into (1.1a)–(1.1c), we find that the remainder terms $(u_r,\mathbf{q}_r)$ solve (4.4a)–(4.4c). Here, we used that

$$\begin{aligned} \nabla\cdot\mathbf{q}_s+\nabla\cdot\mathbf{q}_r &= -\kappa\Delta\big(fG\big)+f_r \\ &= \underbrace{-\kappa f\Delta G}_{f\delta_\Lambda \text{ in the sense of distributions}} \underbrace{-2\kappa\nabla f\cdot\nabla G-\kappa\Delta f\,G+f_r}_{=0}. \end{aligned} \tag{4.10}$$

Remark 1. By the superposition principle, the solution splitting (4.1) can be extended to a collection of straight line segments $\Lambda=\cup_i\Lambda_i$. More concretely, this can be achieved by setting

$$G(\mathbf{x}) = \frac{1}{4\pi\kappa}\sum_i \ln\left(\frac{r_{b,i}+L_i+\boldsymbol{\tau}_i\cdot(\mathbf{a}_i-\mathbf{x})}{r_{a,i}+\boldsymbol{\tau}_i\cdot(\mathbf{a}_i-\mathbf{x})}\right) \tag{4.11}$$

while keeping $(u_s,\mathbf{q}_s)$ as was defined in (4.2) and $(u_r,\mathbf{q}_r)$ as defined by (4.4a)–(4.4c) and (4.5a)–(4.5b). Here, $\mathbf{a}_i,\mathbf{b}_i$ denotes the endpoints of line segment Λ_i, $r_{b,i}=\mathrm{dist}(\mathbf{x},\mathbf{b}_i)$ and $r_{a,i}=\mathrm{dist}(\mathbf{x},\mathbf{a}_i)$ the distance from its endpoints, $L_i=\|\mathbf{b}_i-\mathbf{a}_i\|$ the line segment length, and $\boldsymbol{\tau}_i$ its normalized tangent vector.

Remark 2. The explicit construction of the function G in (4.9) requires Λ to be a straight line segment. For more general lines, Λ could be approximated by a set of line segments Λ_i, and G could be constructed approximately by (4.11). Alternatively, it is possible to base the construction of G on a curvilinear coordinate system wherein Λ coincides with a coordinate line and subsequently transform the resulting expression back to $\mathbb{R}^3$.

4.2. Regularity of the splitting terms. The key point of the solution splitting (4.1) is that it forms a split into lower- and higher-regularity terms. In this section, we will discuss in more detail the regularity of the splitting terms. In particular, we will show that for $0 < \alpha < 1$,

$$(u_s, \mathbf{q}_s) \in L^2_{\alpha-1}(\Omega) \times V_{\alpha+1}(\mathrm{div}; \Omega), \tag{4.12a}$$

$$(u_r, \mathbf{q}_r) \in L^2(\Omega) \times H(\mathrm{div}; \Omega). \tag{4.12b}$$

We start by showing (4.12a). As the singular terms in the splitting are explicitly given using the function G, this can be done by straightforward calculation. Formally, G contains a logarithmic-type singularity and a ∇G a r^{-1}-type singularity in the plane normal to Λ. We refer here to our earlier work in [21, section 3.2], where the precise regularity of G was determined using weighted Sobolev spaces. Therein, it was found that

$$G \in L^2_{\alpha-1}(\Omega), \quad \nabla G \in (L^2_\alpha(\Omega))^3, \quad \text{and } \partial_s G \in L^2(\Omega). \tag{4.13}$$

As f was assumed to belong to $C^2(\bar{\Omega})$, it then follows directly that

$$u_s \in L^2_{\alpha-1}(\Omega) \text{ and } \mathbf{q}_s \in L^2_\alpha(\Omega). \tag{4.14}$$

Finally, a calculation of $\nabla \cdot \mathbf{q}_s$ shows that $\nabla \cdot \mathbf{q}_s = 0$ a.e. The exception is at $r = 0$, wherein it admits a r^{-2}-type singularity. The divergence of $\mathbf{q}_s$ therefore belongs to $L^2_{\alpha+1}(\Omega)$. It follows that $\mathbf{q}_s \in V_{\alpha+1}(\mathrm{div}; \Omega)$.

In order to identify the regularity of $(u_r, \mathbf{q}_r)$, consider the right-hand side f_r in (4.5a). A calculation shows

$$\begin{aligned} \|f_r\|_{L^2(\Omega)} &\leq \kappa \left(\|\Delta f G\|_{L^2(\Omega)} + \|2\nabla f \cdot \nabla G\|_{L^2(\Omega)} \right) \\ &\leq \kappa \|\Delta f\|_{L^\infty(\Omega)} \|G\|_{L^2(\Omega)} + 2\kappa \|\nabla f\|_{L^\infty(\Omega \setminus \Omega_\epsilon)} \|\nabla G\|_{L^2(\Omega \setminus \Omega_\epsilon)} \\ &\quad + 2\kappa \|(\partial_s f)(\partial_s G)\|_{L^2(\Omega_\epsilon)} \\ &< \infty, \end{aligned} \tag{4.15}$$

where we used the assumption that there exists $\epsilon > 0$ such that $f = f(s)$ in Ω_ϵ; this implies that the normal and binormal components of ∇f vanish in Ω_ϵ. With $f_r \in L^2(\Omega)$, the existence of $(u_r, \mathbf{q}_r) \in L^2(\Omega) \times H(\mathrm{div}; \Omega)$ solving (4.4a)–(4.4c) then follows by standard elliptic theory; see, e.g., [9].

Remark 3. The requirement on f to be locally constant with respect to s in Ω_ϵ can be relaxed to $f \in C^2(\bar{\Omega})$ by the construction of an extension operator. Let $\tilde{\Lambda}$ denote the elongation of Λ, $\tilde{\Lambda} = \Omega \cap \{\boldsymbol{\tau} s + \mathbf{a} \text{ for } s \in (-\infty, \infty)\}$. For an illustration of this, we refer the reader to Figure 2 in [21]. As $f \in C^2(\bar{\Omega})$, $f|_\Lambda \in C^2(\tilde{\Lambda})$. Let P denote the projection operator $P : \Omega \to \tilde{\Lambda}, \mathbf{x} \to (\mathbf{x} - \mathbf{a}) \cdot \boldsymbol{\tau}$ mapping points $\mathbf{x} \in \Omega$ onto their closest point on $\tilde{\Lambda}$. We then define the extension operator

$$E : C^2(\tilde{\Lambda}) \to C^2(\Omega) \text{ with } E(f)(\mathbf{x}) \to \tilde{f}(P(\mathbf{x})), \tag{4.16}$$

where $\tilde{f}$ denotes some smooth extension of f on $\tilde{\Lambda}$. One then has $E(f) = E(f)(s)$ in Ω_ϵ for some $\epsilon > 0$. A solution splitting of the type (4.1) can then be constructed by switching f with $E(f)$.

5. Discretization. In this section, we will introduce the finite element discretization of the line source problem. We give here two different discretization methods: The first solves directly for the full solution $(u, \mathbf{q})$ via (3.1a)–(3.1b), while the second solves for the remainder pair $(u_r, \mathbf{q}_r)$ using the weak formulation of (4.4a)–(4.4c). Since the remainder pair are of higher regularity than the full solution, we expect this second approach to achieve improved convergence rates.

Assume, for simplicity, the domain Ω to be polyhedral; Ω then readily admits a decomposition $\mathcal{T}_h$ into tetrahedra K,

$$\bar{\Omega} = \bigcup_{K \in \mathcal{T}_h} K,$$

where h denotes the mesh size $h = \max_{K\in\mathcal{T}_h} h_K$ and $\mathcal{T}_h$ is assumed to satisfy all the requirements of a conforming, quasi-uniform mesh. This mesh does not have to conform to Λ. We use piecewise polynomial elements of degree k to approximate u and u_r,

$$\mathbb{DG}_h^k := \{w_h \in L^2(\Omega) : w_h|_K \in P_k(K) \quad \forall\, K \in \mathcal{T}_h\},$$

and the H^{div}-conforming Raviart–Thomas elements of degree k to approximate $\mathbf{q}$ and $\mathbf{q}_r$,

$$\mathbb{RT}_h^k := \{\mathbf{w} \in (L^2(\Omega))^3 : \mathbf{w}_h|_K \in P_{k-1}(K, \mathbb{R}^n) \oplus \mathbf{x}P_{k-1}(K) \quad \forall\, K \in \mathcal{T}_h\}.$$

Here, P_k denotes the standard space of polynomials of degree $\leq k$ with $k \geq 1$ integer valued. The (standard) mixed finite element formulation of (3.1a)–(3.1b) then reads as follows: Find $(u_h, \mathbf{q}_h) \in \mathbb{DG}_h^{k-1} \times \mathbb{RT}_h^k$ such that

$$(\kappa^{-1}\mathbf{q}_h, \mathbf{v}_h) - (\nabla \cdot \mathbf{v}_h, u_h) + (\mathbf{v}_h, u_0)_{\partial\Omega} = 0 \qquad \forall\, \mathbf{v} \in \mathbb{RT}_h^k, \tag{5.1a}$$

$$(\nabla \cdot \mathbf{q}_h, \theta_h) = (f, \theta_h)_\Lambda \qquad \forall\, \theta \in \mathbb{DG}_h^{k-1}. \tag{5.1b}$$

Stability and convergence rates for this formulation are nontrivial to prove, as the solution belongs to the nonstandard space $L^2_{\alpha-1}(\Omega) \times V_{\alpha+1}(\mathrm{div}; \Omega)$. We leave it here as an open question and investigate it only numerically. Let us note, however, that $L^2_{\alpha+1}(\Omega) \not\subset L^1(\Omega)$ and that $\mathbb{DG}_h^{k-1} \not\subset L_{-\alpha-1}(\Omega)$. For this reason, we will now define an alternative solution strategy.

Assuming the assumptions stated in section 4 hold, one can solve for $(u, \mathbf{q})$ via the higher-regularity remainder terms: Find $(u_{r,h}, \mathbf{q}_{r,h}) \in \mathbb{DG}_h^{k-1} \times \mathbb{RT}_h^k$ such that

$$(k^{-1}\mathbf{q}_{r,h}, \mathbf{v}_{r,h}) - (\nabla \cdot \mathbf{v}_{r,h}, u_{r,h}) + (\mathbf{v}_{r,h}, u_{r,0})_{\partial\Omega} = 0 \qquad \forall\, \mathbf{v}_{r,h} \in \mathbb{RT}_h^k, \tag{5.2a}$$

$$(\nabla \cdot \mathbf{q}_{r,h}, \theta_{r,h}) = (f_r, \theta_{r,h}) \quad \forall\, \theta_{r,h} \in \mathbb{DG}_h^k, \tag{5.2b}$$

where the right-hand side f_r and boundary data $u_{r,0}$ are given by (4.5a) and (4.5b), respectively. We will refer to this method as the singularity removal–based mixed finite element method for the line source problem. As $f_r \in L^2(\Omega)$, the stability and convergence properties of (5.2a)-(5.2b) follow from the standard theory of the mixed finite element method. For later discussion, let us note the results. Given $(u_r, \mathbf{q}_r) \in H^k(\Omega) \times (H^{k+1}(\Omega))^3$ and $(u_{r,h}, \mathbf{q}_{r,h}) \in \mathbb{DG}_h^{k-1} \times \mathbb{RT}_h^k$ solving (5.2a)–(5.2b), one has [10, III.3.4, Proposition 3.9]

$$\|u_r - u_{r,h}\|_{L^2(\Omega)} + \|\mathbf{q}_r - \mathbf{q}_{r,h}\|_{H(\mathrm{div};\Omega)} \leq Ch^k \left(\|u_r\|_{H^k(\Omega)} + \|\mathbf{q}_r\|_{(H^{k+1}(\Omega))^3}\right). \tag{5.3}$$

Remark 4. The convergence rate in (5.3) is given with respect to the higher-regularity terms $(u_r, \mathbf{q}_r)$ in the solution splitting (4.1) and their numerical approximation $(u_{r,h}, \mathbf{q}_{r,h})$. Given $(u_{r,h}, \mathbf{q}_{r,h})$, an approximation of the full solution could be constructed as $(u_h, \mathbf{q}_h) = (\mathcal{I}(u_s), \mathcal{I}(\mathbf{q}_s)) + (u_{r,h}, \mathbf{q}_{r,h})$, where $\mathcal{I}$ would denote some interpolation operator. The convergence rates for the approximation $(u_h, \mathbf{q}_h)$ would then depend on the choice of interpolation operator.

6. Numerical results. In this section, we will test the approximation properties of the two discretization methods given in the last section, i.e., the (standard) mixed method (5.1a)–(5.1b) and the singularity removal–based mixed method (5.2a)–(5.2b). The section will proceed as follows. In section 6.1, we compare the convergence properties of the approximation methods. For the standard method, we compute convergence rates with respect to both weighted and unweighted norms. For the singularity removal–based method, we approximate the remainder function, which belongs to the standard $L^2(\Omega) \times H(\mathrm{div}; \Omega)$ spaces; we therefore compute convergence with respect to standard (unweighted) norms. Finally, we illustrate in section 6.2 the effectiveness of the singularity removal–based method in handling data sets with a large number of line segments by using it to treat a data set for the vascular system of a rat tumor.

6.1. Comparison of standard and singularity removal–based mixed finite element methods. The purpose of this section is to numerically investigate the approximation properties of the standard versus singularity removal–based finite element method. Here, the two approximation methods are given by (5.1a)–(5.1b) and (5.2a)–(5.2b), respectively. To this end, we consider the unit cube domain $\Omega = (0, 1)^3$ with a line cutting vertically through its midpoint:

$$\Lambda = \{(0.5, 0.5, z) : z \in (0, 1)\}. \tag{6.1}$$

The domain Ω is discretized using a uniform tetrahedral mesh. We prescribe a manufactured solution

$$u = -\frac{1}{2\pi}\left(\left(z^2 + 1\right)\ln(r) + \frac{1}{2}r^2(1 - \ln(r))\right) \tag{6.2}$$

that solves the line source problem (3.1a)–(3.1b) with permeability $\kappa = 1$, line source intensity $f(z) = z^2 + 1$, flux $\mathbf{q} := -\nabla u$, and Dirichlet boundary conditions given by (6.2). Because the line Λ extends through the domain, u admits a splitting of the type (4.1) with G defined as

$$G = -\frac{1}{2\pi}\ln(r), \tag{6.3}$$

$(u_s, \mathbf{q}_s)$ still defined as in (4.2) and $(u_r, \mathbf{q}_r)$ as the solution of (4.4a)–(4.4c). The singularity removal–based method then solves (5.2a)–(5.2b) with problem parameters

$$f_r = (\Delta f)G + 2\nabla G \cdot \nabla f = -\frac{1}{\pi}\ln(r), \quad u_{r,0} = u_0 - \frac{z^2 + 1}{2\pi}\ln(r) \tag{6.4}$$

for the remainder pair

$$u_r = -\frac{1}{2\pi}r^2(1 - \ln(r)), \quad \mathbf{q}_r = -\nabla u_r. \tag{6.5}$$

The full solutions u and $\mathbf{q}$, along with the splitting terms, are shown in Figure 6.1.

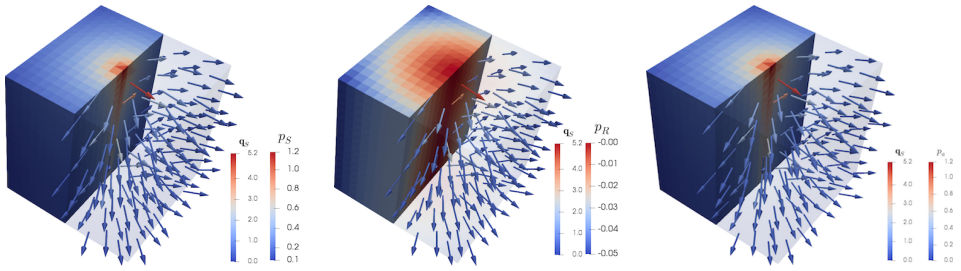

(a) Singular solution components u_s and $\mathbf{q}_s$. (b) Remainder components u_r and $\mathbf{q}_r$. (c) Total solutions $u = u_s + u_r$ and $\mathbf{q} = \mathbf{q}_s + \mathbf{q}_r$.

FIG. 6.1. *The full solutions $u = u_s + u_r$ and $\mathbf{q} = \mathbf{q}_s + \mathbf{q}_r$ and their components to the line source problem* (3.1a)–(3.1b)*, solved on the unit domain with line source intensity $f(z) = z^2 + 1$ and Dirichlet boundary data as in* (6.2).

For the standard finite element method (5.1a)–(5.1b), we want to investigate the error using weighted norms. This requires comparatively fine meshes for the numerical convergence order to be established. For this to be computationally tractable, we fix $z = 1$ so that the problem can be solved on the unit square domain $\Omega = (0, 1)^2$. Restricting our attention to the singular part of the solution,

$$u_s = -\frac{1}{2\pi} f(z = 1) \ln(r), \tag{6.6}$$

we then have a solution of (1.1a)–(1.1c) with right-hand side $f\delta_{\mathbf{x}_0}$. Here, $\delta_{\mathbf{x}_0}$ is a point source centered on $\mathbf{x}_0 = (0.5, 0.5)$, and $f = 2$ is the point source intensity.

Table 6.1 shows the errors and convergence rates obtained using the (standard) mixed finite element method (5.1a)–(5.1b) on this test problem. The variable s gives the numerically computed convergence rate. The errors are given for $\|u - u_h\|$ and $\|\mathbf{q} - \mathbf{q}_h\|$ in the L^2_α-norm for different weights α. Convergence was tested for different element degrees k, with lowest-order $k = 1$ given in Tables 6.1(a) and 6.1(b), $k = 2$ in Tables 6.1(c) and 6.1(d), and $k = 3$ in Tables 6.1(e) and 6.1(f).

Optimal convergence is observed only in Table 6.1(a). The convergence is found to be of order $s = 1$ independently of the weight α, i.e.,

$$\|u - u_h\|_{L^2_\alpha(\Omega)} \leq Ch. \tag{6.7}$$

To understand this result, let us note that the error rate in (5.3) requires $u \in H^1(\Omega)$. In this case, one has $u \in H^1_\alpha(\Omega)$ for any $\alpha > 0$; formally, this can be interpreted as u barely evading $H^1(\Omega)$. Previously, the approximation of this type of problem has been studied in [4] using the conformal finite element method with $\mathbb{P}^1$ elements. Therein, the convergence rate was shown to be of order $h^{1-\epsilon}$ for any $\epsilon > 0$. Applying a similar logic to the mixed finite element method, we formally expect $\|u - u_h\|_{L^2(\Omega)}$ to converge with order $s = 1 - \epsilon$ for arbitrarily small $\epsilon > 0$. As this ϵ is allowed arbitrarily small, the ϵ loss of convergence need not be apparent in the numerical test case.

The remaining convergence rates, conversely, were all found to scale with the error norm weight. The following relationship was observed:

$$\|u - u_h\|_{L^2_\alpha(\Omega)} \leq Ch^{\alpha+1} \tag{6.8}$$

TABLE 6.1

Convergence rates obtained using the (standard) mixed finite element method, as described by (5.1a)–(5.1b)*, measured in the standard ($\alpha = 0$) and weighted L^2_α-norms. The results are given for lowest-order $\mathbb{RT}^1 \times \mathbb{DG}^0$ elements in* (a)–(b), $\mathbb{RT}^2 \times \mathbb{DG}^1$ elements in (c)–(d), and $\mathbb{RT}^3 \times \mathbb{DG}^2$ elements in (e)–(f).

(a) $\|u - u_h\|_{L^2_\alpha(\Omega)}$ with $k = 1$

h \ α	0	0.25	0.5	0.75
16	2.1e-1	2.5e-2	1.6e-2	1.1e-2
32	9.9e-2	1.3e-2	8.2e-3	5.4e-3
64	4.8e-2	6.9e-3	4.1e-3	2.7e-3
128	2.3e-2	3.6e-3	2.1e-3	1.3e-3
s	1.06	0.96	0.99	1.00

(b) $\|\mathbf{q} - \mathbf{q}_h\|_{L^2_\alpha(\Omega)}$ with $k = 1$

h \ α	0.25	0.5	0.75
16	5.1e-1	2.6e-1	1.4e-1
32	4.3e-1	1.9e-1	8.9e-2
64	3.7e-1	1.3e-1	5.4e-2
128	3.1e-1	9.5e-2	3.3e-2
s	0.25	0.50	0.73

(c) $\|u - u_h\|_{L^2_\alpha(\Omega)}$ with $k = 2$

h \ α	0	0.25	0.5	0.75
16	8.3e-2	8.2e-3	3.8e-3	1.8e-3
32	4.0e-2	3.4e-3	1.3e-3	5.6e-4
64	1.9e-2	1.5e-3	4.8e-4	1.7e-4
128	8.8e-3	6.1e-4	1.7e-4	5.0e-5
s	1.08	1.25	1.50	1.73

(d) $\|\mathbf{q} - \mathbf{q}_h\|_{L^2_\alpha(\Omega)}$ with $k = 2$

h \ α	0.25	0.5	0.75
16	5.5e-1	2.5e-1	1.2e-1
32	4.7e-1	1.8e-1	7.0e-2
64	3.9e-1	1.3e-1	4.2e-2
128	3.3e-1	8.9e-2	2.5e-2
s	0.25	0.50	0.75

(e) $\|u - u_h\|_{L^2_\alpha(\Omega)}$ with $k = 3$

h \ α	0	0.25	0.5	0.75
16	4.5e-2	5.2e-3	2.3e-3	1.0e-3
32	2.1e-2	2.2e-3	8.1e-4	3.1e-4
64	1.0e-2	9.2e-4	2.9e-4	9.2e-5
128	4.7e-3	3.9e-4	1.0e-4	2.7e-5
s	1.09	1.25	1.50	1.75

(f) $\|\mathbf{q} - \mathbf{q}_h\|_{L^2_\alpha(\Omega)}$ with $k = 3$

h \ α	0.25	0.5	0.75
16	6.6e-1	2.9e-1	1.3e-1
32	5.5e-1	2.1e-1	7.8e-2
64	4.7e-1	1.5e-1	4.6e-2
128	3.9e-1	1.0e-1	2.8e-2
s	0.25	0.50	0.75

for $k \in \{2, 3\}$ and

$$\|\mathbf{q} - \mathbf{q}_h\|_{L^2_\alpha(\Omega)} \leq Ch^\alpha \tag{6.9}$$

for $k \in \{1, 2, 3\}$. The convergence rate was not found to increase with the polynomial degree k. This is a natural result, as the solutions do not have enough regularity to benefit from higher-order elements. To increase the convergence order, one could instead perform a grading of the mesh, as was proposed in, e.g., [17, 4]. We omit doing that here, as we are interested in solving cases where there are a great number of line sources. It would then be computationally infeasible to perform a mesh refinement around each line segment.

Table 6.2 shows the convergence rates for $\|u_r - u_{r,h}\|$ and $\|\mathbf{q}_r - \mathbf{q}_{r,h}\|$ in different norms. The variable s again gives the numerically computed convergence rate. Only standard (unweighted) norms are used, as the remainder terms u_r and $\mathbf{q}_r$ are not singular. Convergence is tested using element degrees $k \in \{1, 2\}$. As the remainder terms enjoy improved regularity compared to the full solution, we here observe a significant improvement in the convergence rate. To be more precise, we observe here

TABLE 6.2

Convergence rates obtained when solving for the regular terms u_r and $\mathbf{q}_r$ with the mixed finite element method, as described by (5.2a)–(5.2b). *Optimal order convergence is seen in* (a) using $\mathbb{DG}^{k-1} \times \mathbb{RT}^k$ elements with degree $k = 1$.

(a) $k = 1$

h	$\|u_r - u_{r,h}\|_{L^2(\Omega)}$	$\|\mathbf{q}_r - \mathbf{q}_{r,h}\|_{H(\mathrm{div};\Omega)}$
1/2	1.1e-2	1.8e-1
1/4	5.3e-3	9.6e-2
1/8	2.6e-3	5.0e-2
1/16	1.3e-3	2.6e-2
s	1.0	1.0

(b) $k = 2$

h	$\|u_r - u_{r,h}\|_{L^2(\Omega)}$	$\|\mathbf{q}_r - \mathbf{q}_{r,h}\|_{H(\mathrm{div};\Omega)}$
1/2	2.0e-3	3.1e-1
1/4	5.2e-4	1.4e-1
1/8	1.1e-4	6.1e-2
1/16	2.5e-5	2.6e-2
s	2.1	1.2

the convergence rates

$$\|u_r - u_{r,h}\|_{L^2(\Omega)} \leq Ch^k \qquad \text{for } k = 1, 2, \tag{6.10}$$

$$\|\mathbf{q}_r - \mathbf{q}_{r,h}\|_{L^2(\Omega)} \leq Ch \qquad \text{for } k = 1, 2. \tag{6.11}$$

Thus, the approximation converges optimally for lowest-order elements. By calculation, one finds $(u_r, \mathbf{q}_r) \in H^{3-\epsilon}(\Omega) \times (H^{2-\epsilon}(\Omega))^3$ for any $\epsilon > 0$. The error rate is then better than what is expected in (5.3). This can be explained by noting that the solution lies arbitrarily close to $H^3(\Omega) \times (H^2(\Omega))^3$. For the flux $\mathbf{q}_h$, a further increase in the element degree is not seen to increase the convergence. This is to be expected, as $\mathbf{q}$ is not arbitrarily close to $(H^3(\Omega))^3$; thus, it is not regular enough to benefit from this increase in the polynomial degree.

6.2. Convergence test with nontrivial geometry. In the previous section, the singularity removal-based mixed finite element method was found to significantly improve the approximation properties of solutions to (3.1a)–(3.1b). In this section, we will test the capabilities of this method when the line sources are concentrated on a nontrivial geometry. To do so, we consider a data set describing the vascular network in the dorsal skin flap of a rat carcinoma [45]. The skin flap preparation itself has overall dimension of $550 \times 520 \times 230$ μm^3; 106 microvessels were identified within the skin flap, with diameters ranging between 5.0 and 32.2 μm and lengths ranging between 16.0 and 210.1 μm. Due to scale disparities between these values, we therefore consider the skin flap to be a 3D domain Ω and the vascular network to be a 1D graph Λ, as is illustrated in Figure 6.2(a).

As test case, we choose the manufactured solutions

$$u_a = \sum_{i=1}^{106} f_i G_i + \frac{1}{4\pi}\left(r_{\mathbf{b}_i} - r_{\mathbf{a}_i}\right), \quad \mathbf{q}_a = -\nabla u_a \tag{6.12}$$

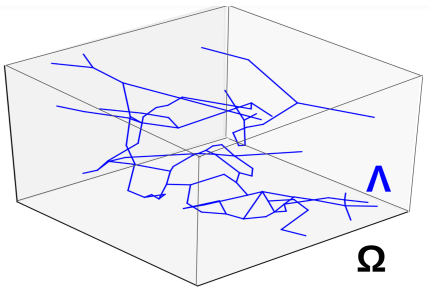

(a) The (3D) simulation domain Ω and the (1D) graph Λ representing the vascular network of a rat tumor.

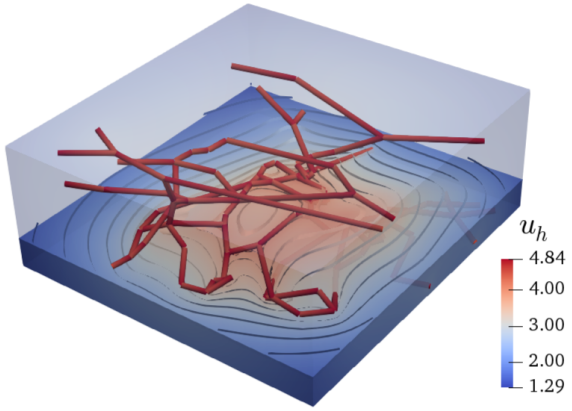

(b) The discretized reconstructed total pressure u_h.

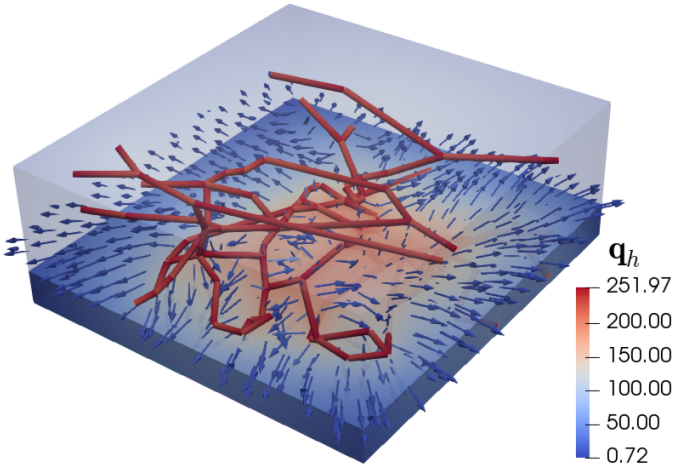

(c) The discretized reconstruction of total flux $\mathbf{q}_h$.

FIG. 6.2. *The pressure* (b) *and flux* (c) *solutions obtained when solving* (1.1a)–(1.1c) *using the singularity removal–based mixed finite element on a problem with nontrivial geometry* Λ.

TABLE 6.3
Error and convergence rates obtained when solving for the regular terms u_r and $\mathbf{q}_r$ on the test problem used in section 6.2.

h	$\|u_{r,a} - u_{r,h}\|_{L^2(\Omega)}$	$\|\mathbf{q}_{r,a} - \mathbf{q}_{r,h}\|_{L^2(\Omega)}$
1/2	5.55e-4	4.50e-3
1/4	2.87e-4	2.28e-3
1/8	1.47e-4	1.12e-3
1/16	7.37e-5	6.17e-4
s	1.0	1.0

with $f_i = 1 + \alpha_i \boldsymbol{\tau}_i \cdot (\mathbf{x} - \mathbf{a}_i)$ for some $\alpha_i \in \mathbb{R}$. By Remark 1, this solution can be split into higher- and lower-regularity terms by defining $(u_r, \mathbf{q}_r)$ as the pair solving (4.4a)–(4.4c) with

$$f_r = \frac{1}{2\pi} \sum_{i=1}^{106} \left(\frac{1}{r_{\mathbf{a}_i}} - \frac{1}{r_{\mathbf{b}_i}} \right), \quad u_{r,0} = \frac{1}{4\pi} \sum_{i=1}^{106} \left(r_{\mathbf{b}_i} - r_{\mathbf{a}_i} \right). \tag{6.13a}$$

The analytic solutions for the remainders are then given by

$$u_{r,a} = \frac{1}{4\pi} \sum_{i=1}^{106} \left(r_{\mathbf{b}_i} - r_{\mathbf{a}_i} \right), \quad \mathbf{q}_{r,a} = -\nabla u_{r,a}. \tag{6.14}$$

Figures 6.2(b) and 6.2(c) show the pressure profile and flux solutions, respectively. Table 6.3 lists the error rates and convergence rates obtained from solving this test problem with the singularity removal–based mixed finite element method with $\mathbb{DG}^0 \times \mathbb{RT}^1$ elements. As in section 6.1, s denotes the numerically computed convergence rate. The convergence rates for $u_{r,h}$ and $\mathbf{q}_{r,h}$ are observed to be of optimal order. Moreover, convergence is obtained using coarse meshes $h = \{1/2, 1/4, 1/8, 1/16\}$. Convergence can evidently be achieved independently of the length scale of Λ.

7. Conclusion. In this work, we have considered the analysis and approximation of the dual-mixed Poisson problem posed in a (3D) domain with a (1D) line source in the right-hand side. The pressure u and flux $\mathbf{q}$ solving this problem are well known to be singular due to the dimensional gap between domain and source term. We showed that the solutions of this problem exist in suitably weighted Sobolev spaces, where the L^2-norms are weighted by the distance to the line; this allows the solution to be singular on the line itself. The flux solution $\mathbf{q}$ was found to require a non-Muckenhoupt weight function for its divergence; in particular, we have $\nabla \cdot \mathbf{q} \in L^2_{\alpha+1} \not\subset L^1(\Omega)$ for $0 < \alpha < 1$.

Approximating the solution with a mixed finite element method shows that the flux fails to converge in the standard (unweighted) L^2-norm. To deal with this, we use a splitting of the solution into higher- and lower-regularity terms to define a singularity removal–based mixed finite element method where only the higher-regularity term is approximated. This method is shown to yield significantly improved convergence rates; in particular, it yields optimal convergence rates for lowest-order Raviart–Thomas elements on quasi-uniform grids.

REFERENCES

[1] I. AAVATSMARK AND R. A. KLAUSEN, *Well index in reservoir simulation for slanted and slightly curved wells in 3d grids*, SPE J., 8 (2003), pp. 41–48.

[2] M. Ainsworth and J. T. Oden, *A Posteriori Error Estimation in Finite Element Analysis*, John Wiley & Sons, New York, 2000.
[3] R. Al-Khoury, P. G. Bonnier, and R. B. J. Brinkgreve, *Efficient finite element formulation for geothermal heating systems. Part* I: *Steady state*, Internat. J. Numer. Methods Engrg., 63 (2005), pp. 988–1013.
[4] T. Apel, O. Benedix, D. Sirch, and B. Vexler, *A priori mesh grading for an elliptic problem with Dirac right-hand side*, SIAM J. Numer. Anal., 49 (2011), pp. 992–1005.
[5] T. Arbogast and A. Taicher, *A linear degenerate elliptic equation arising from two-phase mixtures*, SIAM J. Numer. Anal., 54 (2016), pp. 3105–3122.
[6] I. Babuška and M. B. Rosenzweig, *A finite element scheme for domains with corners*, Numer. Math., 20 (1972), pp. 1–21.
[7] T. Bærland, M. Kuchta, and K.-A. Mardal, *Multigrid methods for discrete fractional Sobolev spaces*, SIAM J. Sci. Comput., 41 (2019), pp. A948–A972.
[8] C. Bernardi, C. Canuto, and Y. Maday, *Generalized inf-sup conditions for Chebyshev spectral approximation of the Stokes problem*, SIAM J. Numer. Anal., 25 (1988), pp. 1237–1271.
[9] D. Braess, *Finite Elements: Theory, Fast Solvers, and Applications in Solid Mechanics*, 3rd ed., Cambridge University Press, Cambridge, 2007.
[10] F. Brezzi and M. Fortin, eds., *Mixed and Hybrid Finite Element Methods*, Springer, New York, 1991.
[11] Z. Cai and C. R. Westphal, *A weighted h(div) least-squares method for second-order elliptic problems*, SIAM J. Numer. Anal., 46 (2008), pp. 1640–1651.
[12] L. Cattaneo and P. Zunino, *A computational model of drug delivery through microcirculation to compare different tumor treatments*, Int. J. Numer. Methods Biomed. Eng., 30 (2014), pp. 1347–1371.
[13] D. Cerroni, F. Laurino, and P. Zunino, *Mathematical analysis, finite element approximation and numerical solvers for the interaction of* 3*D reservoirs with* 1*D wells*, Int. J. Geomath., 10 (2019), https://doi.org/10.1007/s13137-019-0115-9.
[14] L. Chen, M. J. Holst, and J. Xu, *The finite element approximation of the nonlinear Poisson–Boltzmann equation*, SIAM J. Numer. Anal., 45 (2007), pp. 2298–2320.
[15] C. D'Angelo, *Finite element approximation of elliptic problems with Dirac measure terms in weighted spaces: Applications to one- and three-dimensional coupled problems*, SIAM J. Numer. Anal., 50 (2012), pp. 194–215.
[16] C. D'Angelo and A. Quarteroni, *On the coupling of* 1*d and* 3*d diffusion-reaction equations: Application to tissue perfusion problems*, Math. Models Methods Appl. Sci., 18 (2008), pp. 1481–1504.
[17] Y. Ding and L. Jeannin, *A new methodology for singularity modelling in flow simulations in reservoir engineering*, Comput. Geosci., 5 (2001), pp. 93–119.
[18] Q. Fang, S. Sakadzić, L. Ruvinskaya, A. Devor, A. M. Dale, and D. A. Boas, *Oxygen advection and diffusion in a three-dimensional vascular anatomical network*, Opt. Express., 16 (2008), pp. 17530–17541.
[19] I. Gansca, W. Bronsvoort, G. Coman, and L. Tambulea, *Self-intersection avoidance and integral properties of generalized cylinders*, Computer Aided Geom. Design, 19 (2002), pp. 695–707.
[20] I. G. Gjerde, K. Kumar, and J. M. Nordbotten, *A singularity removal method for coupled* 1*d–*3*d flow models*, Comput. Geosci., 24 (2019), pp. 443–457.
[21] I. G. Gjerde, K. Kumar, J. M. Nordbotten, and B. Wohlmuth, *Splitting method for elliptic equations with line sources*, ESAIM Math. Model. Numer. Anal., 53 (2019), pp. 1715–1739.
[22] L. Grinberg, E. Cheever, T. Anor, J. R. Madsen, and G. E. Karniadakis, *Modeling blood flow circulation in intracranial arterial networks: A comparative* 3*d/*1*d simulation study*, Ann. Biomed. Eng., 39 (2011), pp. 297–309.
[23] E. Hodneland, X. Hu, and J. M. Nordbotten, *Well-Posedness, Discretization and Preconditioners for a Class of Models for Mixed-Dimensional Problems with High Dimensional Gap*, preprint, arXiv:2006.12273, 2020.
[24] K. E. Holter, M. Kuchta, and K.-A. Mardal, *Sub-Voxel Perfusion Modeling in Terms of Coupled* 3*d*-1*d Problem*, preprint, arXiv:1803.04896, 2018.
[25] M. Javaux, T. Schröder, J. Vanderborght, and H. Vereecken, *Use of a three-dimensional detailed modeling approach for predicting root water uptake*, Vadose Zone J., 7 (2008), https://doi.org/10.2136/vzj2007.0115.
[26] T. Kilpeläinen, *Weighted Sobolev spaces and capacity*, Ann. Acad. Sci. Fenn. Ser. A I Math., 19 (1994), pp. 95–113.
[27] T. Koch, K. Heck, N. Schröder, H. Class, and R. Helmig, *A new simulation framework for soil–root interaction, evaporation, root growth, and solute transport*, Vadose Zone J., 17 (2018), https://doi.org//10.2136/vzj2017.12.0210.

[28] T. Koch, M. Schneider, R. Helmig, and P. Jenny, *Modeling tissue perfusion in terms of* 1*d*-3*d embedded mixed-dimension coupled problems with distributed sources*, J. Comput. Phys., 410 (2020), 109370.
[29] V. A. Kondratiev and O. Oleinik, *Boundary-value problems for partial differential equations in non-smooth domains*, Russ. Math. Surv., 38 (1983), pp. 1–86.
[30] T. Köppl, E. Vidotto, B. I. Wohlmuth, and P. Zunino, *Mathematical modelling, analysis and numerical approximation of second order elliptic problems with inclusions*, in Numerical Mathematics and Advanced Applications ENUMATH 2015, Springer, New York, 2016.
[31] T. Köppl, E. Vidotto, and B. Wohlmuth, *A local error estimate for the Poisson equation with a line source term*, in Numerical Mathematics and Advanced Applications ENUMATH, Springer, New York, 2016, pp. 421–429.
[32] T. Köppl, E. Vidotto, B. Wohlmuth, and P. Zunino, *Mathematical modeling, analysis and numerical approximation of second-order elliptic problems with inclusions*, Math. Models Methods Appl. Sci., 28 (2018), pp. 953–978.
[33] V. A. Koslov, V. G. Mazya, and J. Rossman, *Elliptic Boundary Value Problems in Domains with Point Singularities*, Math. Surveys Monogr., Vol. 52, Amer. Math. Soc., Providence, RI, 1997.
[34] M. Kuchta, M. Nordaas, J. C. G. Verschaeve, M. Mortensen, and K.-A. Mardal, *Preconditioners for saddle point systems with trace constraints coupling* 2*d and* 1*d domains*, SIAM J. Sci. Comput., 38 (2016), pp. B962–B987.
[35] A. Kufner, *Weighted Sobolev Spaces*, John Wiley & Sons, New York, 1993.
[36] F. Laurino and P. Zunino, *Derivation and analysis of coupled PDEs on manifolds with high dimensionality gap arising from topological model reduction*, ESAIM Math. Model. Numer. Anal., 53 (2019), pp. 2047–2080.
[37] A. A. Linninger, I. G. Gould, T. Marinnan, C.-Y. Hsu, M. Chojecki, and A. Alaraj, *Cerebral microcirculation and oxygen tension in the human secondary cortex*, Ann. Biomed. Eng., 41 (2013), pp. 2264–2284.
[38] A. Llau, L. Jason, F. Dufour, and J. Baroth, *Finite element modelling of* 1*d steel components in reinforced and prestressed concrete structures*, Eng. Struct., 127 (2016), pp. 769–783.
[39] V. Mazya and J. Rossmann, *Elliptic Equations in Polyhedral Domains*, American Mathematical Society, Providence, RI, 2010.
[40] J. N. McDonald and N. A. Weiss, *International Edition: A Course in Real Analysis*, Vol. 2, Elsevier, New York, 1999.
[41] M. Nabil and P. Zunino, *A computational study of cancer hyperthermia based on vascular magnetic nanoconstructs*, R. Soc. Open Sci., 3 (2016), 160287.
[42] D. Notaro, L. Cattaneo, L. Formaggia, A. Scotti, and P. Zunino, *A Mixed Finite Element Method for Modeling the Fluid Exchange between Microcirculation and Tissue Interstitium*, Springer, Cham, Switzerland, 2016, pp. 3–25.
[43] L. Possenti, G. Casagrande, S. D. Gregorio, P. Zunino, and M. Constantino, *Numerical simulations of the microvascular fluid balance with a non-linear model of the lymphatic system*, Microvasc. Res., 122 (2019), pp. 101–110.
[44] J. Reichold, M. Stampanoni, A. L. Keller, A. Buck, P. Jenny, and B. Weber, *Vascular graph model to simulate the cerebral blood flow in realistic vascular networks*, J. Cereb. Blood Flow Metab., 29 (2009), pp. 1429–1443, PMID: 19436317.
[45] T. Secomb, R. Hsu, M. Dewhirst, B. Klitzman, and J. Gross, *Analysis of oxygen transport to tumor tissue by microvascular networks*, Int. J. Radiat. Oncol. Biol. Phys., 25 (1993), pp. 481–489.
[46] B. O. Turesson, *Nonlinear Potential Theory and Weighted Sobolev Spaces*, Springer, Berlin, 2000.
[47] E. Vidotto, T. Koch, T. Köppl, R. Helmig, and B. Wohlmuth, *Hybrid models for simulating blood flow in microvascular networks*, Multiscale Model. Simul., 17 (2019), pp. 1076–1102.
[48] C. J. Weiss, *Finite-element analysis for model parameters distributed on a hierarchy of geometric simplices*, Geophysics, 82 (2017), pp. E155–E167.
[49] C. Wolfsteiner, L. J. Durlofsky, and K. Aziz, *Calculation of well index for nonconventional wells on arbitrary grids*, Comput. Geosci., 7 (2003), pp. 61–82.